nature medicine

Simultaneous PET-MRI reveals brain function in activated and resting state on metabolic, hemodynamic and multiple temporal scales

Hans F Wehrl[1], Mosaddek Hossain[1], Konrad Lankes[1,2], Chih-Chieh Liu[1], Ilja Bezrukov[1,3], Petros Martirosian[4], Fritz Schick[4], Gerald Reischl[1] & Bernd J Pichler[1]

© 2013 Nature America, Inc. All rights reserved.

Combined positron emission tomography (PET) and magnetic resonance imaging (MRI) is a new tool to study functional processes in the brain. Here we study brain function in response to a barrel-field stimulus simultaneously using PET, which traces changes in glucose metabolism on a slow time scale, and functional MRI (fMRI), which assesses fast vascular and oxygenation changes during activation. We found spatial and quantitative discrepancies between the PET and the fMRI activation data. The functional connectivity of the rat brain was assessed by both modalities: the fMRI approach determined a total of nine known neural networks, whereas the PET method identified seven glucose metabolism–related networks. These results demonstrate the feasibility of combined PET-MRI for the simultaneous study of the brain at activation and rest, revealing comprehensive and complementary information to further decode brain function and brain networks.

The study of brain function is of the utmost interest for basic research and clinical diagnostics. Two different imaging modalities are primarily employed to examine brain activity: fMRI, which uses blood oxygen level–dependent (BOLD) contrasts[1], and PET[2]. However, the BOLD effect reflects the complex interactions of blood oxygenation and cerebral metabolic rate of oxygen ($CMRO_2$), cerebral blood flow (CBF) and cerebral blood volume (CBV) changes; all of these interactions are convoluted into a single fMRI signal[3,4]. The recent discovery of default-mode networks in the brain that can be measured by fMRI[5] has further enhanced the field of neuroimaging but has also brought about new unknowns regarding the physiological basis of neuroimaging techniques[6]. Because of its high sensitivity and its ability to track particular biochemical processes based on specific radiolabeled biomarkers, PET is an excellent tool for elucidating the metabolic basis of the fMRI signal and providing complementary information. For example, in the case of the PET tracer 2-[^{18}F]fluoro-2-deoxy-D-glucose ([^{18}F]FDG), glucose metabolism in the brain can be assessed and quantified as cerebral metabolic rate of glucose (CMRGlc).

Comparative measurements between MRI and PET brain activation often suffer from the inability to simultaneously acquire data[7,8]. With recent advances in multimodal imaging, the feasibility of combined PET-MRI in small animals[9] and humans[10] has been demonstrated; however, this new technique has not previously been used to compare brain function between these two modalities by acquiring multiparametric data that are highly spatially and temporally correlated.

The aim of this study is to demonstrate the potential of combined PET-MRI as a tool to investigate brain function on multiple time and metabolic scales. The PET tracer [^{18}F]FDG is able to quantify not only changes in brain activity that are reflected by increases and decreases in CMRGlc but also the baseline brain activity that stems primarily from excitatory synaptic activity[11] and slower metabolic adaptations that are known as metabolic plasticity[12]. Simultaneous [^{18}F]FDG-PET and BOLD-fMRI acquisitions therefore allow the study of neuronal activity using both PET, which provides glucose-metabolic-level data on a slow time scale (minutes) using a sustained stimulus, and fMRI, which provides vascular-level data and information about oxygen metabolism on a fast time scale (seconds) using a block-design stimulus. We extract in addition functional connectivity information from BOLD-fMRI and dynamic [^{18}F]FDG-PET data by performing an independent component analysis (ICA). Finally, we discuss the dependencies between glucose metabolism and neurovascular parameters in the brain and the potential of PET-MRI for depicting a multitude of brain networks.

RESULTS

Phantom studies

To test the fMRI capabilities of the combined PET-MRI system, we performed an fMRI quality assurance study that adhered to a modified Function Biomedical Informatics Research Network protocol[13]. A quantitative evaluation of different fMRI stability parameters led to the conclusion that the stability of the combined PET-MRI is sufficient for the performance of fMRI studies (**Supplementary Fig. 1** and **Supplementary Results**).

Rat studies in the activated state

In a group-level analysis of the BOLD-fMRI data ($n = 8$ rats, two scans each), unilateral stimulation of the whisker pad of the rats produced

[1]Werner Siemens Imaging Center, Department of Preclinical Imaging and Radiopharmacy, Eberhard Karls University, Tuebingen, Germany. [2]Bruker BioSpin MRI, Ettlingen, Germany. [3]Max Planck Institute for Intelligent Systems, Tuebingen, Germany. [4]Section on Experimental Radiology, Department of Diagnostic and Interventional Radiology, Eberhard Karls University, Tuebingen, Germany. Correspondence should be addressed to B.J.P. (bernd.pichler@med.uni-tuebingen.de).

Received 26 July 2012; accepted 28 January 2013; published online 25 August 2013; doi:10.1038/nm.3290

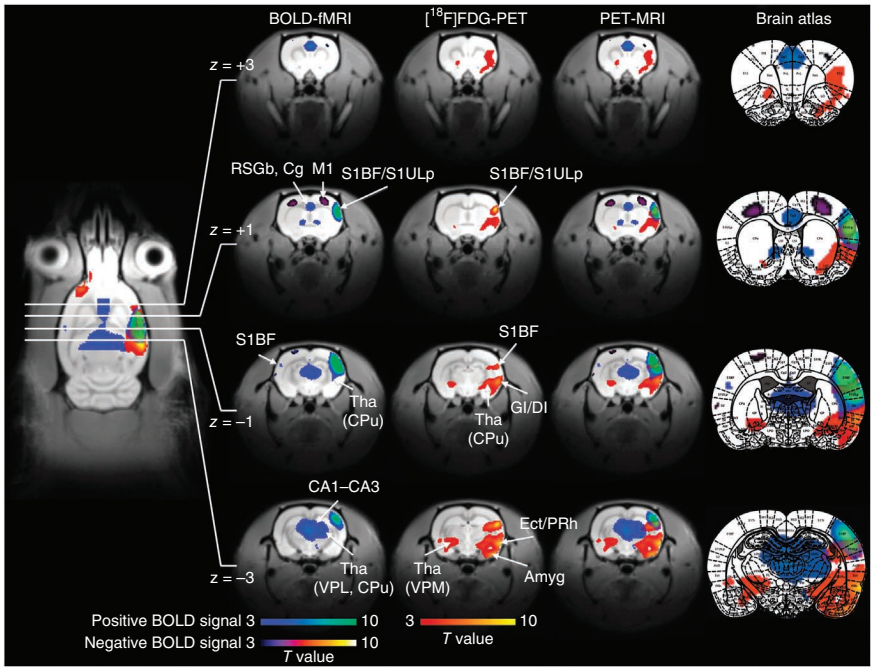

Figure 1 Comparison of PET and fMRI activation. A comparison of activated areas in PET and fMRI, depicting statistically significant ($P < 0.01$) activated areas in colored overlays on the anatomic, grayscale magnetic resonance information identified by simultaneous PET-MRI. In BOLD-fMRI regions with negative BOLD signal are also found. The BOLD-fMRI measurements indicate activation primarily in the contralateral barrel field cortex (S1BF). PET indicated a very strong activation in areas that were not identified by fMRI, such as the amygdala (Amyg), the ectorhinal cortex (Ect) and the perirhinal cortex (PRh), including the insular cortex (GI/DI). The combined PET-MRI activation maps, as presented on both the anatomical structure and the corresponding rat brain atlas sections (reproduced from ref. 16 with permission from Elsevier, copyright 1998) show a mismatch between the activated regions identified by fMRI and PET. Cg, cingulate cortex; Tha, thalamus; CPu, caudate putamen; VPL, ventral posterolateral thalamic nucleus; VPM, ventral posteromedial nucleus; S1ULp, primary somatosensory cortex, upper lip region.

a strong activation of the contralateral whisker barrel field (S1BF, **Fig. 1** and **Table 1**). The contralateral S1BF area is also the area with the fMRI global activation maximum in terms of statistical significance ($P = 4.4 \times 10^{-16}$). Ipsilateral to the stimulation side, we also detected an activation in the S1BF area at nearly the same location ($P = 0.004$); however, this activation was not significant after a family-wise error (FWE) correction. We also observed strong BOLD activation in the contralateral caudate putamen (striatum) and thalamic area ($P = 7.7 \times 10^{-6}$) but not in the ipsilateral striatum ($P = 0.03$), where only a slight activation was identified. The retrosplenial granular cortex (RSGb), including the indusium griseum ($P = 6.4 \times 10^{-10}$) and the cingulate cortex, responded to the stimulation with a strong BOLD signal. In addition, a relatively centrally located area of the brain that included large areas of the hippocampus (for example, CA1–CA3) and stretched downward to the ventral posterolateral thalamic nucleus was activated ($P = 9.2 \times 10^{-7}$). We observed negative BOLD signals in the primary motor cortex (M1), the primary somatosensory cortex forelimb (S1FL) area and somatosensory cortex ($P = 2.1 \times 10^{-4}$, **Supplementary Results**). After a FWE correction at $P < 0.05$, three main activation foci in the contralateral S1BF, the RSGb and cingulate cortex and the central brain area were identified, as were areas with negative BOLD signal in the bilateral M1 and S1FL regions.

The simultaneously acquired PET activation data, using [^{18}F]FDG as a marker for brain glucose consumption, revealed several additional activated areas (for example, the insula and amygdala) that are, in part of their spatial location and function, complementary to the activated areas that were identified using the BOLD-fMRI (**Fig. 1**). We observed the PET global activation maximum in the contralateral S1BF ($P = 3.2 \times 10^{-6}$). However, we did not observe substantial activation in the ipsilateral S1BF ($P > 0.05$). Another hot spot was located in the contralateral ectorhinal cortex and the perirhinal cortex ($P = 1.7 \times 10^{-5}$); this hot spot included the dysgranular and granular insular cortices. Areas of the amygdala, including the amygdalohippocampal area and the posterolateral cortical amygdaloid nucleus, had strong contralateral activation ($P = 3.2 \times 10^{5}$) but also showed a smaller activation on the ipsilateral side ($P = 0.004$). In addition, the contralateral striatal area showed PET activation in the thalamus and caudate putamen ($P = 6.3 \times 10^{-4}$) and in the ventral posteromedial thalamic nucleus ($P = 6.7 \times 10^{-4}$); these regions were less activated on the ipsilateral side ($P = 0.02$). We did not find any areas with substantially less glucose consumption during the stimulation as compared to baseline. The activation in the contralateral S1BF cluster, including the ectorhinal cortex, the dysgranular and granular insular cortices, the amygdala, and the thalamus and caudate putamen, was significant after FWE correction ($P_{FWE} = 0.0024$). For measurements regarding limits in spatial resolution, please refer to the **Supplementary Table 1** and **Supplementary Results**.

Table 1 Activated areas in [^{18}F]FDG-PET–BOLD-fMRI

Modality	Brain area	Coordinates (mm)			P value	T value
		x	y	z		
fMRI positive	S1BF cl	5.9	–3.2	–0.7	4.4×10^{-16}	22.4
	S1BF il	–6.1	–3.4	–0.9	3.6×10^{-4}	3.4
	Tha (CPu cl)	4.9	–5.9	–1.7	7.7×10^{-6}	4.3
	Tha (CPu il)	–4.9	–5.9	1.7	3.3×10^{-2}	1.8
	RSGb, Cg	–0.1	–4.7	–3.2	6.4×10^{-10}	6.1
	CA1–CA3	0.6	–5.1	–1.9	9.2×10^{-7}	4.8
fMRI negative	S1FL cl	3.2	–1.9	1.8	8.9×10^{-8}	5.2
	S2 il	–7.4	–5.0	–1.5	2.1×10^{-4}	3.6
PET	S1BF cl	6.0	–3.3	–3.4	3.2×10^{-6}	12.0
	Ect, PRh	6.9	–7.3	–2.8	1.7×10^{-5}	9.3
	Amyg cl	5.0	–9.9	–3.8	3.2×10^{-5}	8.5
	Amyg il	–4.4	–9.4	–4.6	4.4×10^{-3}	3.6
	Tha (CPu cl)	4.2	–6.8	–2.0	6.3×10^{-4}	5.2
	Tha (VPM cl)	3.0	–8.0	–3.7	6.7×10^{-4}	5.1
	Tha (VPM il)	–3.0	–7.0	–2.8	2.0×10^{-2}	4.2

Areas of significant positive and negative BOLD-fMRI response and increased [^{18}F]FDG-PET uptake measured during whisker stimulation. The values reported in the table are the coordinates (in the Paxinos system, with *z* relative to the bregma) of the peak activation centers with the corresponding *P* values and the *T* values. Cg, cingulate cortex; cl, contralateral; CPu, caudate putamen; Ect, ectorhinal cortex; il, ipsilateral; PRh, perirhinal cortex; S2, secondary somatosensory cortex; Tha, thalamus; VPM, ventral posteromedial nucleus.

© 2013 Nature America, Inc. All rights reserved.

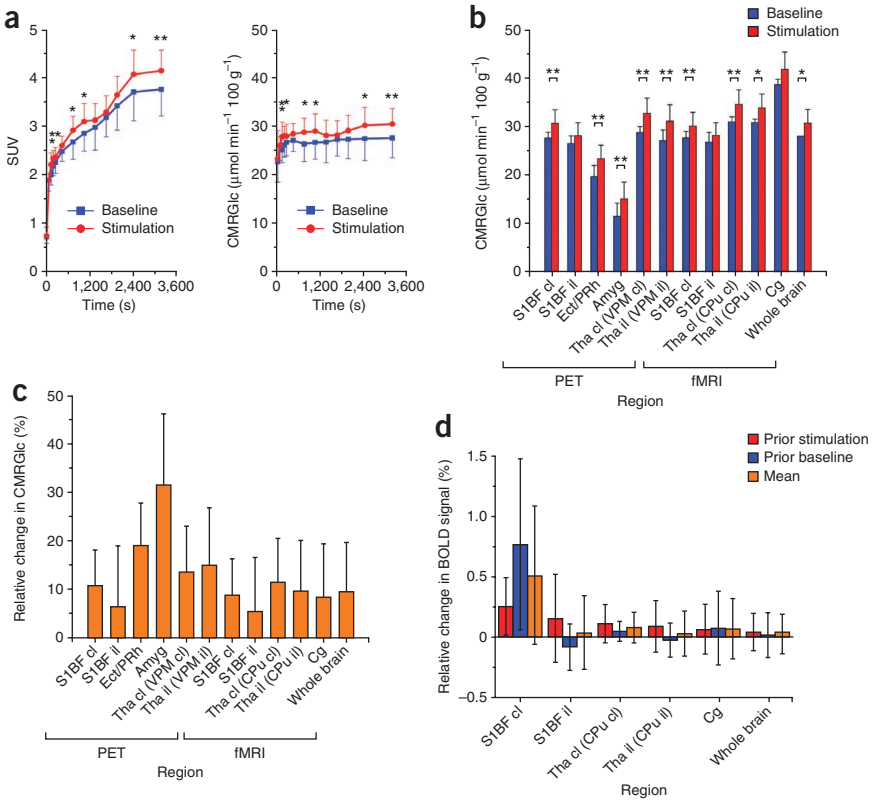

Figure 2 Quantification of PET-MRI stimulus response. (**a**) Averaged ($n = 8$) PET time-curve of the standardized uptake value (SUV) in the contralateral barrel field cortex (cl S1BF) giving a measure of tracer activity in the brain and the corresponding cerebral metabolic rate for glucose (CMRGlc). The highest statistical significance ($P = 0.002$) is achieved using the last 15 min of the 1 h [^{18}F]FDG-PET acquisition. (**b**) Volume-of-interest (VOI) analysis indicates that the PET regions, on average, demonstrated highly significant (**$P < 0.01$) relative changes in CMRGlc compared to the baseline values. The fMRI VOIs show highly significant or significant (*$P < 0.05$) relative changes in CMRGlc in certain cases. (**c**) Average relative change in glucose metabolism, as assessed by PET. (**d**) Relative BOLD signal changes are on average approximately 0.5% in the S1BF. Amyg, amygdala; Cg, cingulate cortex; CPu, caudate putamen; Ect, ectorhinal cortex; il, ipsilateral; PRh, perirhinal cortex; Tha, thalamus; VPM, ventral posteromedial nucleus. The error bars represent ± one standard deviation from multiple animal ($n = 8$) experiments.

The spatial extent of the activated areas (**Fig. 1**) and the location of the peak activation centers differ between the two modalities, with an average distance of 2.7 ± 0.7 mm between the peak contralateral S1BF activation centers for the fMRI and PET observations (**Supplementary Results**). A comparison between the averaged BOLD-fMRI data sets with sustained stimulation and baseline did not reveal any substantial activation in the areas reported above (**Supplementary Fig. 2** and **Supplementary Results**).

Quantification of glucose metabolism and oxygenation changes

Analysis of the PET time curves of the contralateral S1BF (**Fig. 2a**) revealed that time points with a statistical difference between baseline and stimulation states are predominantly either in the first minutes ($t = 150$ s, $P = 0.005$) or toward the end of the 1-h scanning period. We found the largest statistical significant difference between these states in the last 15 min of PET scanning ($t = 3{,}150$ s, $P = 0.002$). The highest standardized uptake value, relating uptake to both injected dose and body weight of the rats, was also reached in this period in the contralateral S1BF, indicating the best signal-to-noise ratio of the PET scans.

The CMRGlc in the investigated volumes of interest (VOIs) was evaluated relative to a CMRGlc of 28.1 μmol min^{-1} 100 g^{-1} for the resting whole brain[14]. CMRGlc values are reported for VOIs based on the activated areas found in fMRI and PET (**Fig. 2b**). CMRGlc (**Fig. 2c**) increased, relative to the respective baseline value of the region, in the contralateral S1BF by an average of 11% ± 7% ($P = 0.005$)

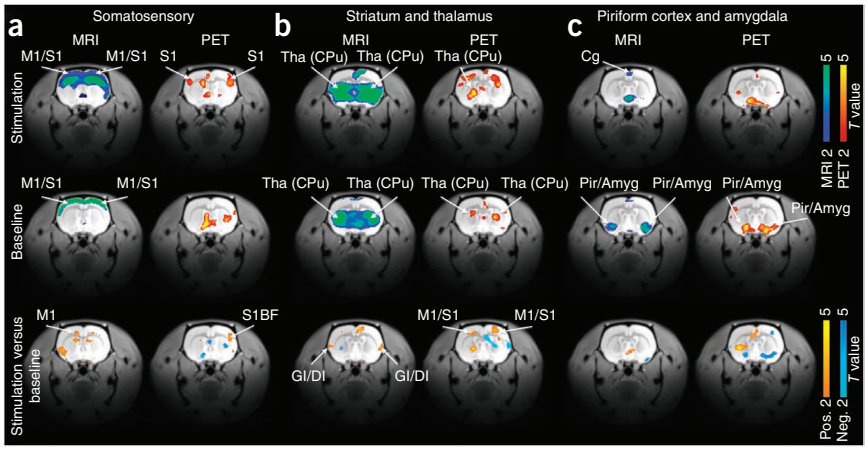

Figure 3 PET-MRI functional connectivity. Example of the major brain networks, as identified by an independent component analysis (ICA) of BOLD-fMRI and dynamic PET data. (**a**) Connectivity was identified in the motor and primary somatosensory cortex (M1/S1, $z = 1$), where a bilateral activity during both stimulation and rest is observed in fMRI. However, the corresponding PET ICA component indicates only a network in the primary somatosensory cortex (S1) area, which is intermixed with activity in the caudate putamen (CPu). (**b**) The same tendency is observed for the striatal and thalamus (Tha) (CPu) regions ($z = 0$), where the fMRI ICA again indicates larger network areas. The differences between stimulation and baseline fMRI ICA show a region in the granular and dysgranular insular cortex (GI/DI) which is consistent with the findings from the PET activation study. (**c**) Finally, the piriform cortex and the amygdala (Pir/Amyg, $z = 0$) show strong functional connectivity both in the fMRI-derived maps and in the PET charts. The MRI and PET representations of the piriform cortex and amygdala components shift more centrally toward the midline of the brain ($x = 0$, nucleus of the vertical limb of the diagonal band) during stimulation. A comparison between sustained stimulus and baseline shows areas where the stimulus signal is larger than the baseline (pos.) and where the stimulus signal is smaller than the baseline (neg.).

© 2013 Nature America, Inc. All rights reserved.

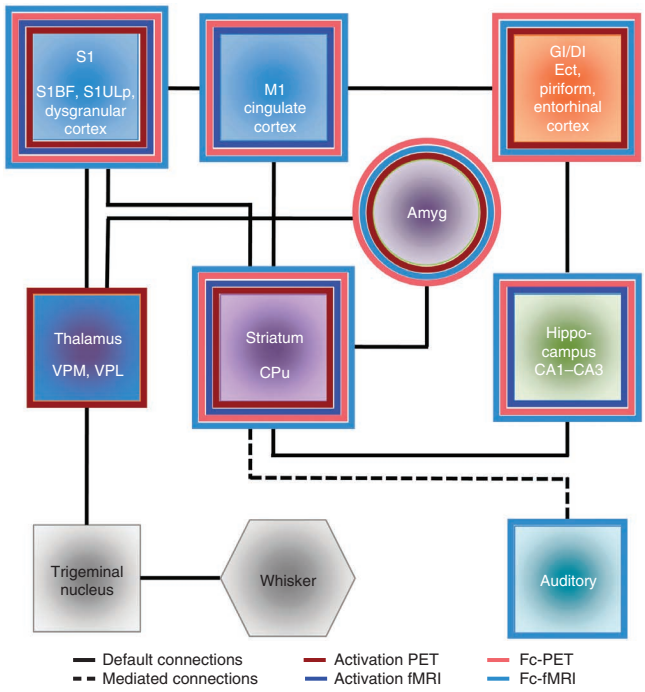

Figure 4 Networks in the whisker system. Major neuronal connections in the whisker system. A multitude of brain regions are involved when applying the whisker stimuli used in this study. Default connections are shown between the different brain regions. Many networks in the brain were observed by fc-fMRI and fc-PET, as indicated by different frame colors. Thalamus and striatum need to be considered together, given the limited imaging resolution of the modalities used. This information emphasizes the complementary structure of combined PET-MRI. CPu, caudate putamen; Ect, ectorhinal cortex; GI/DI, dysgranular and granular insular cortices; VPL, ventral posterolateral thalamic nucleus; VPM, ventral posteromedial nucleus; S1ULp, primary somatosensory cortex, upper lip region.

and in the contralateral amygdala by an average of 32% ± 14% ($P = 2.3 \times 10^{-4}$). In contrast to the relative changes that were observed in the CMRGlc, which ranged from 5% to 32%, the BOLD-fMRI signal alterations were one order of magnitude smaller and only 0.5 ± 0.6% in the contralateral S1BF (**Fig. 2d**, **Supplementary Figs. 3** and **4** and **Supplementary Results**).

Functional connectivity in stimulated and baseline states

Many studies in resting-state BOLD-fMRI make use of the ICA technique to identify different brain networks. ICA was applied to 15-min fMRI acquisitions performed during rest and during stimulation of the animals and to dynamic PET data (**Supplementary Figs. 5** and **6**). A total of nine neuronal circuits, described in the functional connectivity fMRI (fc-fMRI) literature[15], could be identified on the basis of the fMRI data, whereas the PET method yielded seven networks (**Supplementary Table 2**). Several of the functional networks showed inter-relationships in the results of the ICA with other networks and were represented in multiple ICA components (**Supplementary Results**). On the basis of the ICA, we observed strong functional networks (**Fig. 3**) in the somatosensory (S1) and M1 cortices, the striatum and thalamus, and the piriform cortex and amygdala. The area of the ipsilateral S1 and M1 was significantly more activated during sustained stimulation ($x = -1.9$, $y = -2.3$, $z = 1.6$, with x, y and z values given indicating coordinates in units of mm in the Paxinos system[16], with z relative to the bregma; $P = 0.003$, $T_{14} = 3.3$) compared to baseline, whereas we observed stronger connections within this network, as reflected by higher T values, generally during baseline conditions (**Fig. 3a**). The corresponding PET component indicated much smaller regions during activation in the S1 that are bilaterally connected (contralateral: $x = 5.1$, $y = -3.7$, $z = 0.6$, $P = 0.003$ and $T_7 = 4.0$; ipsilateral: $x = -5.3$, $y = -3.2$, $z = -0.2$; $P = 3.0 \times 10^{-4}$ and $T_7 = 5.6$). During baseline, this bilateral network appears to be absent in the PET ICA data. However, a comparison between the activation and baseline PET ICA revealed the contralateral S1BF area ($x = 5.2$, $y = -3.2$, $z = 1.4$; $P = 9.0 \times 10^{-4}$, $T_{14} = 3.8$), which has already been observed in the static PET image analysis in the activated state. The striatal areas demonstrated strong bilateral networks during both stimulation and rest conditions in fMRI (**Fig. 3b**). During stimulation, these areas stretch toward the dysgranular and granular insular cortices, whereas they are more confined to the striatum and thalamus during baseline conditions. We also observed bilateral caudate putamen areas in the corresponding PET ICA during baseline conditions (contralateral: $x = 1.7$, $y = -5.7$, $z = 1.3$; $P = 1.5 \times 10^{-7}$, $T_7 = 18.9$, ipsilateral: $x = -1.4$, $y = -4.8$, $z = -0.5$; $P = 2.8 \times 10^{-4}$, $T_7 = 6.0$) but found a stronger unilateral focus during activation. Finally, we could observe the piriform cortex and the area of the amygdala in both the MRI and PET ICA components, and we saw stronger bilateral characterization of these regions in the baseline images (**Fig. 3c**).

We have assessed a multitude of activated brain regions and functional connectivities using combined PET-MRI imaging. The different areas that we observed in the respective modalities indicate the complementarities of the PET-MRI data (**Fig. 4**).

DISCUSSION

We found a mismatch between PET and fMRI stimulation data. The BOLD-fMRI activation areas, which are primarily in the contralateral S1BF, are in accordance with previously performed electrical and air whisker-stimulation experiments[17,18]. The PET activation that is found in S1BF corresponds to areas that were previously identified in the literature either without detailed quantification[19] or in animals that were killed before PET acquisition[20].

Although the brain regions that are identified by fMRI are primarily involved in somatosensory circuits, the regions observed with PET also encompass areas such as the insula, the thalamus or the amygdala that are known to be involved in, for example, pain processing, emotion and attention. Therefore the PET-observable regions are complementary in terms of their function to the primary contralateral S1BF activation found in BOLD-fMRI. This phenomenon is potentially caused by the effects of the different stimulus durations that are used for the MRI and PET measurements. The PET stimulus was permanently applied for 45 min and therefore represents a sustained stimulus, whereas the MRI stimulus was switched on only for 30-s time blocks. At least for high stimulus intensities, it has been demonstrated in humans that stimuli of longer durations produce higher pain ratings[21]. After checking for physiological indications of pain, we found that neither a short nor a sustained application of the stimulus used in this study showed clear signs of nociception in the rats (**Supplementary Fig. 7** and **Supplementary Discussion**). The PET data observed in this study are further supported by experiments that show an increase in insula and thalamic activation with increased stimulus duration but not with perceived stimulus intensity[22]. The combined PET-MRI measurements in this study indicate two main networks: the somatosensory network, which is primarily imaged by BOLD-fMRI, and the network that relates to higher-order functions

© 2013 Nature America, Inc. All rights reserved.

evoked by the stimulus, such as emotion, attention and nociceptive processing, which is revealed by PET (**Fig. 4**). We did not observe the additional areas found by PET when we performed a sustained-stimulus BOLD-fMRI analysis.

A spatial and geometric mismatch between a BOLD-fMRI and a corresponding PET activation focus is expected because these two methods measure brain function on the basis of different physiological processes. The signal for gradient-echo BOLD sequences, in particular, is more heavily weighted toward the draining veins and macro vessels[23]. The [^{18}F]FDG-PET signal, by contrast, arises at late time points, primarily from the tissue compartment, and possesses a relatively low activity concentration in blood[24].

Our quantitative values for the relative changes of CMRGlc and BOLD-fMRI signal during stimulation are in the range reported in the literature, although different stimulation currents and anesthesia protocols have been used in previously published studies[7,25]. Also the use of different PET and fMRI image normalization procedures and anesthetics can affect quantification (**Supplementary Figs. 8** and **9** and **Supplementary Discussion**).

We observed a mismatch between BOLD-fMRI and CMRGlc signals in certain brain regions, indicating a complementary nature of both methods. PET and fMRI methods are sensitive to different components of the metabolic-hemodynamic coupling. [^{18}F]FDG-PET is a surrogate marker for glucose metabolism[26], and BOLD-fMRI arises from a complex interplay of hemodynamic parameters, including CBF, CBV and $CMRO_2$ (ref. 27). Our results suggest that in some areas of the brain, for example, the amygdala, the BOLD signal changes might be too slow and too small to be detected (**Supplementary Discussion**). Hence, in these cases, [^{18}F]FDG-PET provides a more sensitive measure for brain activation. Further PET-MRI studies using the capability to observe multiple metabolic scales (for example, [^{18}F]FDG-PET and lactate magnetic resonance spectroscopy) could help to clarify these issues (**Supplementary Discussion**).

We performed functional connectivity analysis on the basis of fMRI and PET data. The components identified by the MRI measurement correspond well to the networks that have been observed in the literature[15]. To our knowledge, our approach to extract functional connectivity information from dynamic PET data using ICA has not been shown previously. We were able to identify seven networks that show similarities with networks described in the fMRI-literature[15] using this new technique. However, in general, the areas found in PET ICA are smaller compared to the regions assigned in fc-fMRI (**Supplementary Discussion**). The fc-PET data do not show the distinctive bilateral patterns that are observed in fc-fMRI. Similarly to the case with fc-PET, unilateral patterns of functional connectivity networks in the brain have been observed with fc-fMRI in mice[15] and rats[28]. The observation of fc-PET networks that are similar to fc-fMRI networks indicates that fundamental information about brain networks is coded in dynamic PET data, which are largely unused by conventional image analysis methods. Areas of elevated aerobic glycolysis correlating with the brain networks identified by fc-fMRI have been shown in humans[29]. Our results now reveal that the temporal dynamics of glucose consumption is region dependent and connected to fc-fMRI networks.

There is sufficient evidence for neural contributions to fc-fMRI measurements[30], but the sources of the fc-fMRI signal are still under investigation[6]. Our ICA analysis of the fc-PET data indicates a temporal correlation between various brain regions; seven of these networks were described in the fc-fMRI literature[15]. However, given that the nature of fc-fMRI is still not fully understood and given the scarcity of studies involving fc-PET, the possibility of an underlying functional connectivity remains to be proven. Further studies are needed to validate and clarify the role of fc-PET also with respect to the components observed not matching the fc-fMRI networks and to determine whether it can provide complementary information to fc-fMRI.

To the best of our knowledge, the experiments and findings described herein constitute the first small-animal brain activation study to be performed using simultaneous PET-MRI. We have proven that the functional brain activation data of small animals can be acquired *in vivo* using a small-animal PET insert. We visualized changes in blood oxygenation and hemodynamics by fMRI, whereas we monitored metabolic adaptations of glucose consumption by [^{18}F]FDG-PET, revealing different networks within the brain (**Fig. 4**). The functional connectivity analysis of dynamic brain PET data shows similarities to the networks discovered by fc-fMRI. We expect that the further potential of this multimodal technique can be assessed by use of PET tracers such as [^{15}O]H_2O for perfusion or [^{11}C]raclopride for receptor occupation. PET-MRI is an excellent tool that can be used to explore and potentially help to explain the enigmatic nature of the BOLD signal in activated and resting states, especially if the techniques described in this study are further extended to include CBF, CBV and $CMRO_2$ measurements. Our study clearly shows that an interplay between multiple techniques and disciplines is needed to further enhance knowledge about how the brain works.

METHODS

Methods and any associated references are available in the online version of the paper.

Note: Any Supplementary Information and Source Data files are available in the online version of the paper.

ACKNOWLEDGMENTS

We thank F. Cay and M. Koenig for excellent technical support during this project. This study was supported by the German Research Foundation (Deutsche Forschungsgemeinschaft PI 771/1-1, PI 771/5-1), the Wilhelm Schuler-Foundation and the Werner Siemens-Foundation.

AUTHOR CONTRIBUTIONS

H.F.W. and B.J.P. designed the study, evaluated and analyzed data and prepared the manuscript, H.F.W., M.H., K.L., C.-C.L., I.B. and B.J.P. developed the PET insert, G.R. produced the radiotracer, H.F.W. and M.H. made PET-MRI measurements, H.F.W., P.M. and F.S. developed the MRI sequence, and all authors read and edited the manuscript.

COMPETING FINANCIAL INTERESTS

The authors declare competing financial interests: details are available in the online version of the paper.

Reprints and permissions information is available online at http://www.nature.com/reprints/index.html.

1. Ogawa, S., Lee, T.M., Kay, A.R. & Tank, D.W. Brain magnetic resonance imaging with contrast dependent on blood oxygenation. *Proc. Natl. Acad. Sci. USA* **87**, 9868–9872 (1990).
2. Phelps, M.E. & Mazziotta, J.C. Positron emission tomography: human brain function and biochemistry. *Science* **228**, 799–809 (1985).
3. Buxton, R.B. Interpreting oxygenation-based neuroimaging signals: the importance and the challenge of understanding brain oxygen metabolism. *Front. Neuroenergetics* **2**, 8 (2010).
4. Logothetis, N.K. What we can do and what we cannot do with fMRI. *Nature* **453**, 869–878 (2008).
5. Biswal, B.B., Van Kylen, J. & Hyde, J.S. Simultaneous assessment of flow and BOLD signals in resting-state functional connectivity maps. *NMR Biomed.* **10**, 165–170 (1997).
6. Zhang, D. & Raichle, M.E. Disease and the brain's dark energy. *Nat. Rev. Neurol.* **6**, 15–28 (2010).

© 2013 Nature America, Inc. All rights reserved.

7. Shih, Y.Y., Wey, H.Y., De La Garza, B.H. & Duong, T.Q. Striatal and cortical BOLD, blood flow, blood volume, oxygen consumption, and glucose consumption changes in noxious forepaw electrical stimulation. *J. Cereb. Blood Flow Metab.* **31**, 832–841 (2011).
8. Kinahan, P.E. & Noll, D.C. A direct comparison between whole-brain PET and BOLD fMRI measurements of single-subject activation response. *Neuroimage* **9**, 430–438 (1999).
9. Judenhofer, M.S. *et al.* Simultaneous PET-MRI: a new approach for functional and morphological imaging. *Nat. Med.* **14**, 459–465 (2008).
10. Schlemmer, H.P. *et al.* Simultaneous MR/PET imaging of the human brain: feasibility study. *Radiology* **248**, 1028–1035 (2008).
11. Hjornevik, T. *et al.* Metabolic plasticity in the supraspinal pain modulating circuitry after noxious stimulus-induced spinal cord LTP. *Pain* **140**, 456–464 (2008).
12. Magistretti, P.J. Neuron-glia metabolic coupling and plasticity. *J. Exp. Biol.* **209**, 2304–2311 (2006).
13. Wehrl, H.F. *et al.* Assessment of MR compatibility of a PET insert developed for simultaneous multiparametric PET/MR imaging on an animal system operating at 7 T. *Magn. Reson. Med.* **65**, 269–279 (2011).
14. Shimoji, K. *et al.* Measurement of cerebral glucose metabolic rates in the anesthetized rat by dynamic scanning with 18F-FDG, the ATLAS small animal PET scanner, and arterial blood sampling. *J. Nucl. Med.* **45**, 665–672 (2004).
15. Jonckers, E., Van Audekerke, J., De Visscher, G., Van der Linden, A. & Verhoye, M. Functional connectivity fMRI of the rodent brain: comparison of functional connectivity networks in rat and mouse. *PLoS ONE* **6**, e18876 (2011).
16. Paxinos, G. & Watson, C. *The Rat Brain in Sterotaxic Coordinates* (Academic Press, San Diego, 1998).
17. Kennerley, A.J., Mayhew, J.E., Redgrave, P. & Berwick, J. Vascular origins of BOLD and CBV fMRI signals: statistical mapping and histological sections compared. *Open Neuroimag. J.* **4**, 1–8 (2010).
18. Sanganahalli, B.G., Herman, P. & Hyder, F. Frequency-dependent tactile responses in rat brain measured by functional MRI. *NMR Biomed.* **21**, 410–416 (2008).
19. Kornblum, H.I. *et al. In vivo* imaging of neuronal activation and plasticity in the rat brain by high resolution positron emission tomography (microPET). *Nat. Biotechnol.* **18**, 655–660 (2000).
20. Ravasi, L. *et al.* Use of [^{18}F]fluorodeoxyglucose and the ATLAS small animal PET scanner to examine cerebral functional activation by whisker stimulation in unanesthetized rats. *Nucl. Med. Commun.* **32**, 336–342 (2011).
21. Koyama, Y., Koyama, T., Kroncke, A.P. & Coghill, R.C. Effects of stimulus duration on heat induced pain: the relationship between real-time and post-stimulus pain ratings. *Pain* **107**, 256–266 (2004).
22. Tran, T.D., Wang, H., Tandon, A., Hernandez-Garcia, L. & Casey, K.L. Temporal summation of heat pain in humans: evidence supporting thalamocortical modulation. *Pain* **150**, 93–102 (2010).
23. Yu, X. *et al.* Direct imaging of macrovascular and microvascular contributions to BOLD fMRI in layers IV–V of the rat whisker-barrel cortex. *Neuroimage* **59**, 1451–1460 (2012).
24. Backes, H. *et al.* Whiskers area as extracerebral reference tissue for quantification of rat brain metabolism using ^{18}F-FDG PET: application to focal cerebral ischemia. *J. Nucl. Med.* **52**, 1252–1260 (2011).
25. Bosshard, S.C. *et al.* Assessment of brain responses to innocuous and noxious electrical forepaw stimulation in mice using BOLD fMRI. *Pain* **151**, 655–663 (2010).
26. Fox, P.T., Raichle, M.E., Mintun, M.A. & Dence, C. Nonoxidative glucose consumption during focal physiologic neural activity. *Science* **241**, 462–464 (1988).
27. Kim, S.G. & Ogawa, S. Biophysical and physiological origins of blood oxygenation level-dependent fMRI signals. *J. Cereb. Blood Flow Metab.* **32**, 1188–1206 (2012).
28. Hutchison, R.M., Mirsattari, S.M., Jones, C.K., Gati, J.S. & Leung, L.S. Functional networks in the anesthetized rat brain revealed by independent component analysis of resting-state FMRI. *J. Neurophysiol.* **103**, 3398–3406 (2010).
29. Vaishnavi, S.N. *et al.* Regional aerobic glycolysis in the human brain. *Proc. Natl. Acad. Sci. USA* **107**, 17757–17762 (2010).
30. Fox, M.D. & Raichle, M.E. Spontaneous fluctuations in brain activity observed with functional magnetic resonance imaging. *Nat. Rev. Neurosci.* **8**, 700–711 (2007).

© 2013 Nature America, Inc. All rights reserved.

ONLINE METHODS

PET-MRI. We performed the phantom and small-animal imaging studies on a 7-T animal magnetic resonance scanner (ClinScan, Bruker) with an installed PET insert that was developed and built up in our laboratory (**Supplementary Methods**).

Phantom studies. Please see the **Supplementary Methods**.

Animal experiments. All of the rat experiments were performed in accordance with an animal use and care protocol that was approved by the local authorities (Regierungspraesidium Tuebingen Animal Use and Care Committee). We used eight healthy Lewis male rats (388 ± 29 g, Charles River Laboratories). The rats were fasted for a period of 12 h before the experiments but had access to water *ad libitum*.

Rat *in vivo* PET-MRI imaging. We imaged the rats ($n = 8$) with simultaneous PET-MRI on two consecutive days. For magnetic resonance image acquisition, a linearly polarized RF coil 72 mm in diameter (Bruker) for transmission was used in combination with a four-channel rat brain coil (Bruker) for reception. For simultaneous PET-MRI acquisition, we installed our large field of view (FOV) PET insert inside the magnetic resonance scanner, as described in greater detail in the **Supplementary Methods**. The rats were kept under anesthesia (1.2% isoflurane evaporated in air during the measurements) and maintained at a body temperature of 37 ± 1 °C with a temperature feedback system (Medres). We placed an intravenous (i.v.) catheter in the tail vein of the rats, with tubing of 0.8 m in length (dead volume 62.5 μL) allowing access to the i.v. line inside the PET-MRI bore. We measured blood glucose levels immediately before the experiment. We placed a pair of subcutaneous needle electrodes (SA Instruments) in the left whisker pad of the rats and connected them to a stimulus generator (Multi Channel Systems). Using magnetic resonance localizer images, each rat was centered with its brain inside the PET-MRI FOV. We administered an i.v. injection of 39 ± 3 MBq of [^{18}F]FDG and started at the same time a 60-min dynamic PET scan and a 45-min permanent stimulation of the whiskers (3 mA, 3 Hz and pulse width 500 μs) (**Supplementary Fig. 10**). The experiment was repeated on a consecutive day without the 45-min permanent stimulation period. Four rats were stimulated for 45 min on day 1 and were assessed without stimulation on day 2 to obtain baseline measurements, whereas another set of four rats was subjected to baseline measurements on day 1 and stimulation on day 2 to avoid any bias in the data acquisition with respect to the order of measurement events. Therefore, we performed a total of eight baseline and eight stimulation scans. The magnetic resonance data were acquired concurrently with the PET acquisition (see **Supplementary Methods** for details about the magnetic resonance protocols).

Data processing. For phantom studies, we converted the magnetic resonance data into the NIFTI (Neuroimaging Informatics Technology Initiative) format. Further processing and analysis were performed using MATLAB (R2010b, The MathWorks) programs that were written in-house and that adhered to a modified Function Biomedical Informatics Research Network (FBIRN) protocol[13]. For rat experiments, we converted PET and magnetic resonance images into the NIFTI format and processed them further using statistical parametric mapping (SPM8, Wellcome Trust Center for NeuroImaging). Volume-of-interest (VOI) analyses were performed in SPM8, using the MarsBaR Region of Interest Toolbox (MarsBaR version 0.43, available at http://marsbar.sourceforge.net/). We analyzed the resting-state data using the Group ICA Toolbox (GIFT 2.0, MIND Research Network). The combined PET-MRI population atlas (**Supplementary Fig. 11**) was matched to the Paxinos space[16]. We provide the coordinates in units of millimeters, with the x axis running lateral to the midline with negative coordinates representing positions to the left of the midline (the stimulation side) and positive coordinates representing positions to the right of the midline, the y coordinate indicating the ventral position relative to the bregma and the z coordinate representing the anterior (positive) or posterior (negative) position relative to the bregma. We report the coordinates of the nearest local T value maxima if not otherwise specified. More details on the data processing can be found in the **Supplementary Methods**.

Statistical analyses. We used SPM8 to calculate three-dimensional T maps of BOLD-fMRI and PET data (**Supplementary Methods**). For the statistical analysis of VOI data, we employed a paired Student's t-test for the comparison of PET values between the stimulation and baseline measurements in the same subjects and checked homogeneity of the data using Levene's test in combination with the Welch test. A two-tailed Student's t-test was performed to compare the phantom study data and also for the BOLD signal response data. We used Origin 8 (OriginLab) and spreadsheet software to determine significance levels. The data are shown as the means ± s.d. The phantom experiments were performed in triplicate, and the rat experiments were performed with $n = 8$ rats. P values <0.05 were considered to be statistically significant.

Additional methods. The detailed methodology is described in the **Supplementary Methods**.

© 2013 Nature America, Inc. All rights reserved.